

Synthesis, Characterization, and Biofuel Application of Mesoporous Zirconium Oxophosphates

Swapan K. Das,[†] Manas K. Bhunia,[†] Anil K. Sinha,[‡] and Asim Bhaumik^{*,†}

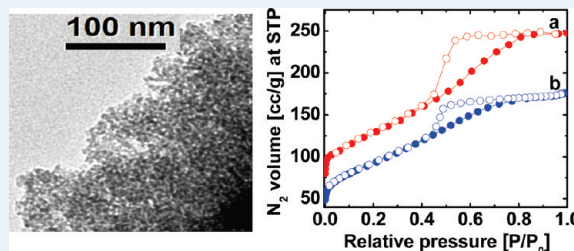
[†]Department of Materials Science, Indian Association for the Cultivation of Science, Jadavpur, Kolkata 700 032, India

[‡]Catalytic Conversion and Process Development Division, Indian Institute of Petroleum, Dehradun 248 005, India

S Supporting Information

ABSTRACT: Mesoporous zirconium oxophosphates have been synthesized through the evaporation-induced self-assembly (EISA) method in the presence of an amphiphilic block copolymer, pluronic F127 as template under strongly acidic conditions. The mesophases of the materials were analyzed by using small-angle powder X-ray diffractions and transmission electron microscopic (TEM) image analysis. N₂ adsorption–desorption studies showed high surface area (260–312 m² g⁻¹) and narrow pore size distribution (4.5–5.5 nm) for the materials. NH₃-TPD and pyridine-IR analyses suggested the presence of strong Lewis and Brønsted acid sites. These mesoporous materials showed excellent catalytic activity in biodiesel reaction for the effective conversion of the long chain fatty acids to their respective methyl esters. The maximum biodiesel yield was about 91% under optimal reaction conditions. High catalytic activity could be attributed to the large surface area and the presence of large number of acidic sites located at the surface of the materials. The catalysts showed negligible loss of activity after five repetitive cycles.

KEYWORDS: mesoporous, zirconium oxophosphate, biodiesel, fatty acid, esterification



1. INTRODUCTION

Open framework porous materials have attracted a great deal of interests over the years because of their potential as green adsorbent and catalysts, which could resolve the environmental concern and waste management.^{1–3} Mesoporous materials can fulfill this area owing to their distinctive properties like high surface area, uniform pore size distribution (PSD), plenty of well distributed active sites,^{4–6} and ease of diffusion for large reacting molecules through their channels.^{7,8} Functionalized porous solids have been employed as heterogeneous catalysts because they are environmentally green with respect to corrosiveness, nonhazardous in nature, and offer ease of catalyst recovery and reusability.^{7,9–12} Solid acid catalysts can be used in biodiesel production, which is an environment-friendly fuel as it is made from renewable resources and low cost feedstocks, like yellow greases, rendered animal fats, and trap greases that contain a significant concentration of free fatty acids. It is usually derived from the esterification of free fatty acids or the transesterification of triglycerides with methanol or ethanol.^{13,14} Industrial trans-esterification processes using homogeneous base catalysts are associated with higher production cost for biodiesel manufacture because of neutralization and separation problems.¹⁵

Moreover, the base catalyzed process suffers from some limitations of feedstock. The contents of free fatty acid in the feedstock need to be lower than 0.5 wt %, otherwise soap formation seriously hinders the production of biodiesel.¹⁶ Esterification is thus needed for converting long-chain free fatty acids into esters. Esterifications are conventionally catalyzed under homogeneous conditions using concentrated sulfuric acid, which

is corrosive and poor for waste discharge.¹⁷ Thus solid acid catalysts are preferable, which could eliminate the corrosion problems and offer easy separation of catalysts from the products through simple filtration. For solid acid catalysts, the carboxylic acid first adsorbs on the catalytic site, and this is followed by reaction with the alcohol from the bulk phase.^{18–20} To date, several groups have developed various solid acids for the esterification of long chain fatty acids; these include zeolites,^{21–23} sulfonated carbonized sugar,^{7,8} sulfated zirconia,^{21,22} sulfated silica-zirconia,²⁴ functional ionic liquid,²⁵ zirconium phosphate supported over different metal oxides,²⁶ and organosulfonic acid mesoporous silica²⁷ and so forth. These solid acids catalyze the esterification of fatty acids with methanol at 453 K. Kiss et al. have also developed another class of interesting biodiesel catalysts such as metal oxides, which include niobic acid, sulfated zirconia, sulfated titania, and sulfated tin oxide.²² Cheng et al. have developed a sulfated zirconia anchored mesoporous silica catalyst for the esterification of long-chain free fatty acids heterogeneously at 341 K in 2007.²⁴

On the other hand the mesoporous metallophosphates have been invented either post-synthesis method or direct method by several group of researchers.^{28,29} Mesoporous zirconium oxophosphate/phosphates have been synthesized through the post-synthesis method by employing CTAB as structure directing agent.^{30,31} Later, Wu and his co-workers have synthesized porous zirconium phosphate through the post-synthesis surface reaction

Received: January 8, 2011

Revised: March 23, 2011

Published: March 25, 2011

between mesoporous zirconium oxide, prepared by using CTAB as surfactant, and phosphoric acid.³² Very recently, Sinhamahapatra et al. have developed mesoporous zirconium phosphate by utilizing CTAB as structure directing agent in aqueous medium with pore dimensions ranging 2–3 nm, which have active acidic sites to catalyze Friedel–Craft benzylation reaction.¹¹ Rao et al. have developed porous zirconium phosphate, which catalyzes esterification reaction of palmitic acid with methanol to only 20% conversion. However, this zirconium phosphate when supported with WO₃ behaves as a strong acid catalyst and convert the palmitic acid to its corresponding ester more efficiently.²⁶

In this context, herein we have developed new mesoporous zirconium oxophosphate materials through the evaporation-induced self-assembly (EISA) method by using non-ionic Pluronic F127 as structure directing agent in acidic nonaqueous medium. These materials possess high surface areas with pore dimensions in the range of large mesopores. To the best of our knowledge fabrication of mesoporous zirconium oxophosphate with large pore dimension by using Pluronic F127 as structure directing agent through the EISA method and their use as heterogeneous solid acid catalyst in biodiesel formation reaction has not been explored. In most of the cases, mesoporous metallophosphates and other known biodiesel catalysts have been synthesized mainly through a post-synthesis method with relatively small pore (2–3 nm) dimension.^{7,8,21–23,32} Furthermore, in all the catalysts prepared by the post-synthesis method the active sites are not easy accessible to the reactants because of the pore blocking and inhomogeneous distribution of active sites, and consequently is responsible for their low reactivity. Here, we have synthesized mesoporous zirconium oxophosphate with large pore (~5.0 nm) and high surface area in one pot, which reduces the probability of pore blocking and inhomogeneity problem. Furthermore, NH₃-TPD analysis suggests the presence of reasonable amount of Lewis and Brønsted acid sites. High surface area together with large pores and presence of strong Lewis and Brønsted acid sites have motivated us to explore the catalytic potential of the mesoporous zirconium oxophosphate materials in biodiesel reaction between different alcohols as well as several long-chain free fatty acids into their corresponding esters. Here large pore dimension favors the diffusion of long chain fatty acid molecules. The materials are characterized thoroughly by using different characterization tools such as powder X-ray diffraction (XRD), transmission electron microscopy (TEM), scanning electron microscopy (SEM)-energy dispersive spectroscopy (EDS), thermogravimetry (TG)-differential thermal analysis (DTA), UV–visible reflectance, and FT IR spectroscopy.

2. EXPERIMENTAL SECTION

2.1. Chemicals. Triblock copolymer poly(ethylene glycol)-*block*-poly(propylene glycol)-*block*-poly(ethylene glycol) (Pluronic F127, $M_{av} = 12600$, EO₁₀₆PO₇₀EO₁₀₆) was used as the structure-directing agent and zirconium(IV) butoxide [Zr(OC₄H₉)₄] were purchased from Sigma-Aldrich. Hydrochloric acid (HCl) and orthophosphoric acid (H₃PO₄) were obtained from Merck. In catalytic reactions different alcohols and fatty acids were used. Cyclohexanol, 2-ethylhexanol were procured from Loba Chemie, benzyl alcohol, methanol from Merck, all fatty acids (lauric acid, myristic acid, palmitic acid, stearic acid) obtained from Loba Chemie and were used without further purification.

2.2. Preparation of Mesoporous Zirconium Oxophosphate (MZrP). In a typical synthesis of mesoporous zirconium oxophosphate, 30 mL absolute ethanol was acidified with 3.30 g (35 wt %) hydrochloric acid. Then 2.0 g triblock copolymer pluronic F127 was added to this acidic ethanol medium and allowed to stir until dissolution. Then 3.84 g (0.01 M) zirconium-(IV) butoxide (taken in 5 mL ethanol) was added slowly under vigorous stirring and allowed to stir for 30 min. During stirring precipitation should be avoided. Then, to this clear solution 1.16 g of (0.01 M) orthophosphoric acid (88 wt %, taken in 5 mL ethanol) was slowly dropwise added under vigorous stirring at ambient temperature. Then the reaction mixture was covered and allowed to stir overnight at room temperature. The mixture was placed inside the oven at 343 K to undergo the EISA process. Finally, the obtained solid sample was calcined through slow increase of the temperature to 773 K (1 K min⁻¹ ramping rate) followed by heating at 773 K for 5 h in the presence of air to obtain template-free mesoporous zirconium oxophosphate. Similarly, two other MZrP samples have been synthesized through the above-mentioned method just by varying the zirconium to phosphorus ratio of 2:1 and 4:1. These three synthesized mesoporous zirconium oxophosphate materials having the zirconium to phosphorus ratio of 1:1, 2:1, and 4:1 are abbreviated as samples 1, 2 and 3, respectively.

3. CHARACTERIZATION TECHNIQUES

Powder XRD of the samples were recorded on a Bruker AXS D-8 Advance diffractometer operated at 40 kV voltage and 40 mA current and calibrated with a standard silicon sample, using Ni-filtered Cu K α ($\lambda = 0.15406$ nm) radiation. TEM images were recorded on a JEOL 2010 TEM operated at 200 kV. A Jeol JEM 6700 field emission scanning electron microscope (FE–SEM) with an energy dispersive X-ray spectroscopic (EDS) attachment was used for the determination of morphology of the particles and its surface chemical compositions, respectively. Nitrogen adsorption/desorption isotherms of the samples were recorded on a Quantachrome Autosorb 1C, at 77 K. Prior to the gas adsorption measurements, the samples were degassed at 423 K for 4 h under high vacuum. Fourier transform infrared (FT IR) spectra of these samples, pyridine adsorption/desorption studies including variable temperature pyridine desorption were recorded on KBr pellets by using Perkin-Elmer Spectrum 100 spectrophotometer. UV–visible diffuse reflectance spectra were recorded on a Shimadzu UV 2401PC with an integrating sphere attachment, and BaSO₄ was used as background standard. Thermogravimetric analysis (TGA) and DTA of the sample were carried out in a TGA instrument thermal analyzer TA-SDT Q-600 under N₂ flow. Temperature programmed desorption of ammonia (TPD-NH₃) was carried out in a Micromeritics Instrument Corporation ChemiSoft Unit 1. In a typical experiment for the TPD measurement, mesoporous zirconium oxophosphate samples 1 and 2 were activated under the flow of He gas at 873 K (3 h) followed by cooling at 298 K and then adsorbing ammonia through injection until complete saturation (observed from the respective thermal conductivity detector (TCD) signal). Physically adsorbed ammonia was then removed by desorbing it in He at 373 K. TPD experiment was then carried out by raising the temperature of the catalyst in a programmed manner (10 deg/min). Areas under the peaks were converted to equivalent ammonia per gram on the basis of injection of known volumes of ammonia at similar conditions.

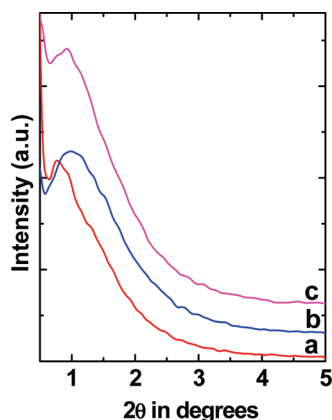


Figure 1. Small-angle powder XRD patterns of mesoporous zirconium oxophosphate (MZrP) samples 1 (a), 2 (b), and 3 (c).

3.1. Catalytic Conditions. Catalytic esterification of different alcohols with acetic acid were carried out in a two neck round-bottom flask fitted with a water condenser and placed in an oil bath at 373 K under magnetic stirring. The temperature of the oil bath was kept constant. During this experiment, acetic acid and different alcohols have been taken in stoichiometric ratio of 3:1, and 3 wt % of catalysts has been taken with respect to alcohol. In a typical run, alcohol and acetic acid have been taken in the mentioned ratio, and a desired amount of catalyst was added immediately into this. Esterification of different fatty acids with a low molecular weight alcohol methanol was carried out at 343 K. In this case 5 wt % of catalyst with respect to fatty acid was used in the reactions. Here the stoichiometric ratio of fatty acid and methanol has been taken as 1:10. In both cases at the selected time intervals the products were collected from the reaction mixtures and analyzed by capillary gas chromatography (Agilent 4890D, FID). Products were identified from known standards and mass spectrometric analysis by using a Micromass Q-tof-Micro Quadrupole mass spectrophotometer. In the esterification reactions of different alcohols the percentage of conversion was estimated by taking the respective alcohol as standard, whereas fatty acids have been taken as standard in the esterification with different fatty acids.

3.2. Reuse of the Catalysts. At the end of the reaction, catalysts were separated from the reaction mixture by filtration and were thoroughly washed with methanol and *n*-hexane or acetone several times to remove both polar and nonpolar compounds that were adsorbed at the surface of the catalysts.³³ After the reaction the catalysts were activated through overnight drying at 343 K followed by 393 K for 4 h and then used as catalyst for recycling experiments. This whole process has been continued five times.

4. RESULTS AND DISCUSSION

4.1. Nanostructure. The small-angle powder XRD patterns for calcined mesoporous zirconium oxophosphate materials are shown in Figure 1. All these samples showed a single intense broad peak with no distinctive higher order peaks in their respective small-angle powder XRD patterns. This single peak in their respective small-angle diffraction pattern corresponds to the characteristic distribution maximum of the nearest-neighbor pore-center-to-pore-center distance between the disordered pores.³⁴ The small-angle peak at 2θ of 0.76° observed for MZrP-1 (sample 1) correspond to an inter-pore separation of 11.61 nm,

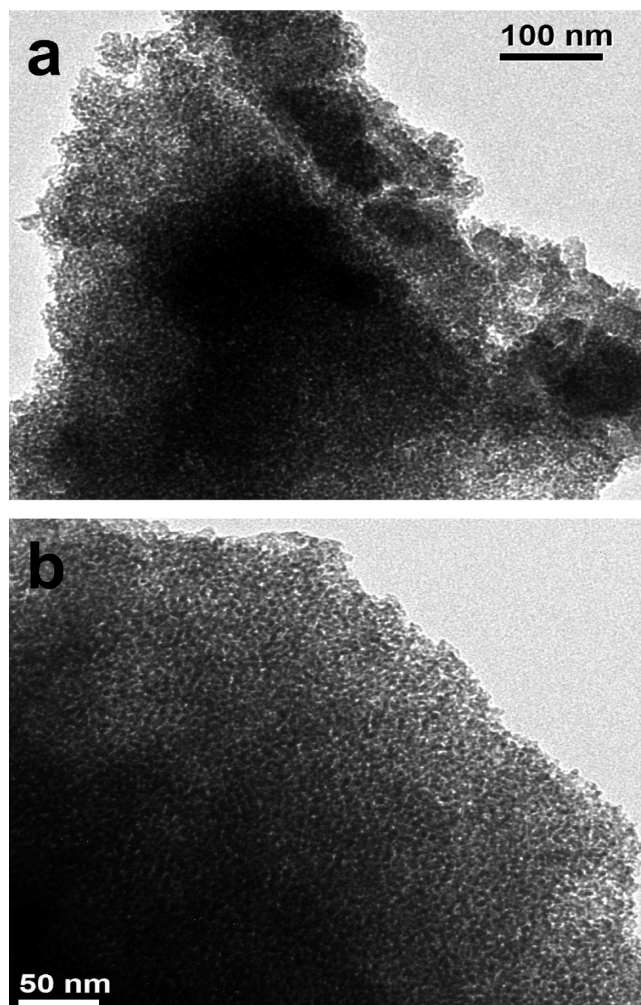


Figure 2. TEM images of samples 1 (a) and 2 (b) seen through the direction perpendicular to the pore axis.

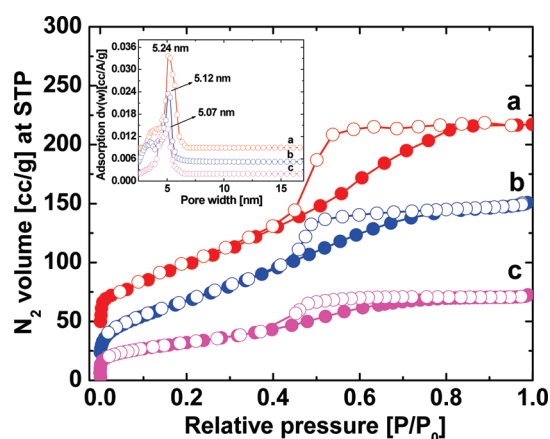


Figure 3. N_2 adsorption/desorption isotherms of samples 1 (a), 2 (b), and 3 (c) measured at 77 K. Adsorption points are marked by filled circles and desorption points by empty circles. Respective NLDFT PSDs are shown in inset.

whereas that for sample 2 small-angle peak observed at 0.98° corresponds to an inter-pore separation of 9.01 nm. Absence of

Table 1. Physico-Chemical Properties of Mesoporous Zirconium Oxophosphate Materials

entry	sample type	surface area (m ² g ⁻¹)	pore width (nm)	pore volume (cc g ⁻¹)
1	Sample 1	312	5.24	0.312
2	Sample 2	241	5.12	0.228
3	Sample 3	116	5.07	0.106
4 ^a	Sample 1	7.6	6.88	0.015
5 ^b	Sample 2	4.7	6.68	0.021

^a Sample 1 calcined at 1173 K. ^b Sample 2 calcined at 1173 K-2. (Respective isotherms are shown in Supporting Information, Figure S4).

further diffraction peaks suggested that pores are arranged more or less disorderly in these materials. The wide-angle powder diffraction patterns of calcined mesoporous zirconium oxophosphate materials at different temperature (773 and 1173 K) are shown in Supporting Information, Figure S1. The XRD patterns at 773 K exhibited only two very broad peaks in the 2θ range of 15–35° and 40–60°, indicative of the amorphous nature of the pore walls. No crystallized ZrPO₄ and/or ZrO₂ phases were detected at this temperature.³⁵ When the materials were calcined at 1173 K, crystallinity was developed, which is confirmed in the wide-angle XRD patterns (Supporting Information, Figure S1). However, surface area is drastically reduced, indicating the collapse of the mesostructure upon high temperature calcination.

4.2. Particle Morphology and Dimensions. Representative TEM images of mesoporous zirconium oxophosphate materials (MZrP) are shown in Figure 2. In images, low electron density spots (pores) are seen throughout the specimen, and the pores are distributed randomly giving a wormhole-like disordered mesostructure. We have measured the interpore separation or pore-to-pore center correlation distance (11.61 and 9.01 nm for samples 1 and 2, respectively) from low-angle powder XRD patterns by using Bragg's law, which include pore dimensions as well as pore-wall thickness.³⁶ N₂ sorption analysis (see below) revealed the pore dimensions, which are typically about 5.0 nm. Thus, the rest of the dimensions, that is, 4.0 to 6.5 nm could contribute to the pore-wall thickness of the mesoporous zirconium oxophosphate samples. FE SEM images of the calcined mesoporous zirconium oxophosphate materials are shown in Supporting Information, Figure S2. As seen from the images that samples are composed of spherical nanoparticles with dimension ranging from 50 to 100 nm.

4.3. Surface Area and Pore Dimensions. Nitrogen adsorption/desorption isotherms and their respective PSDs of the calcined mesoporous zirconium oxophosphate materials are shown in Figure 3 and inset of the Figure 3, respectively. For all these samples the isotherms can be classified as type IV characteristic of mesoporous materials.³⁴ Pronounced desorption hysteresis suggests the existence of large mesopores in these materials. This hysteresis is an intermediate between typical H1 and H2-type hysteresis loop in the P/P_0 range from 0.40 to 0.90 suggesting large uniform mesopores with a cage like pore structure connected by windows with a small size.³⁷ All these samples (Figure 3a and 3b) exhibit broad increase of N₂ uptake in the P/P_0 range from 0.42 to 0.85 clearly indicating that there is a wide range of mesopores within the mesoporous materials. Brunauer–Emmett–Teller (BET) surface area, average pore diameter, and pore volume for calcined MZrP samples are given in Table 1. The respective BET surface area and pore volume of sample 1 were

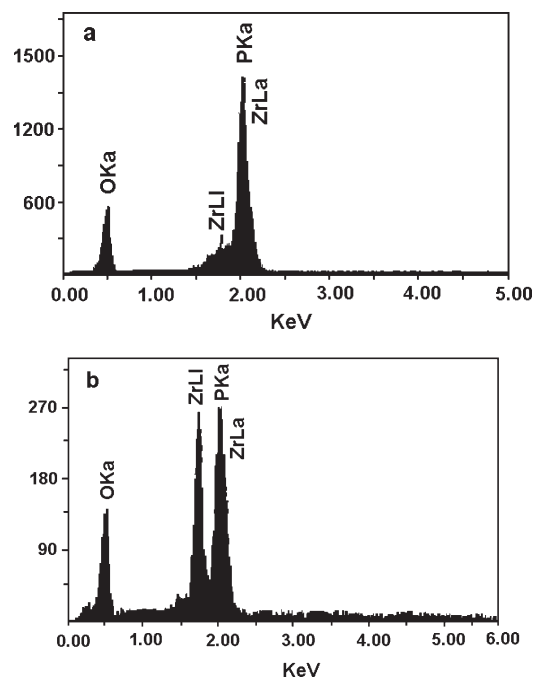


Figure 4. EDS surface chemical analysis of samples 1 (a) and 2 (b).

312 m² g⁻¹ and 0.312 cc g⁻¹, for sample 2 were 241 m² g⁻¹ and 0.228 cc g⁻¹, and for sample 3 were 116 m² g⁻¹ and 0.106 cc g⁻¹ as shown in Table 1. From the surface area analysis it is clear that increasing zirconium to phosphorus ratio reduces both the surface area as well as pore volume. PSD of these samples estimated by employing Non-Local Density Functional Theory (NLDFT) method. Peak pore widths (w) observed are 5.24, 5.12, and 5.07 nm for the samples 1, 2, and 3, respectively. Thus, calcination at 773 K successfully removed the F127 template molecules from the frameworks of as-synthesized materials to generate the mesoporosity. Furthermore, nitrogen adsorption/desorption isotherms and their respective PSDs of the calcined MZrP-1 materials at higher temperature (1173 K) are shown in Supporting Information, Figure S3 and its inset, respectively. From the nature of the isotherms and PSDs it is clear that the nanostructure completely collapsed on high temperature calcinations.

4.4. Chemical Analysis. The EDS patterns and the contents of different elements present in calcined MZrP samples are shown in Figure 4 and Table 2, respectively. The EDS pattern at different positions in the specimen suggested uniform distribution of Zr, P, and O in the samples. In the Figure 4 it is clear that P peak overlaps with the Zr peak for both samples. The molar ratio of P and Zr has been taken as 1:1 during the gel formation for sample 1, whereas after calcination the observed wt % of Zr, P, and O in the mesoporous sample was found to be 41.32, 12.25, and 46.43 wt %, respectively. When the values of wt % are divided by their respective atomic weights and normalized ($Zr + P = 1$), the observed molecular formula is Zr_{0.53}P_{0.47}O_{3.41}.³⁸ Thus, the molar ratio of P and Zr in the calcined sample 1 is 1:0.88. When the molar ratio of P and Zr has been taken in the gel as 1:2, the observed wt % of Zr, P, and O were found to be 45.62, 11.69, and 42.67 wt %, respectively. The estimated molecular formula predicted by using the above procedure is Zr_{0.6}P_{0.4}O_{3.06} and the molar ratio of P and Zr in this framework is 1:1.51.

Table 2. EDS Surface Chemical Analysis of Mesoporous Zirconium Oxophosphate Materials

sample type	elements	(keV)	mass %	error %	atomic %
MZrP-1/Sample 1	O K	0.525	46.43	0.41	77.37
	P K	2.013	12.25	0.13	10.55
	Zr K	2.042	41.32	0.33	12.08
	total		100		100
MZrP-1/Sample 2	O K	0.525	42.67	1.69	75.25
	P K	2.013	11.69	0.55	10.64
	Zr K	2.042	45.64	1.41	14.11
	total		100		100

4.5. Absorption Studies. UV–visible spectroscopy is one of the important tools for characterizing the optical properties as well as the co-ordination modes present in mesoporous zirconium oxophosphate materials. UV–visible diffuse reflectance spectra of calcined MZrP samples showed one broad absorption peak ~ 210 – 220 nm (Supporting Information, Figure S4), which is attributed to the ligand to metal charge transfer transition (LMCT) from the outermost p electrons of oxygen (2p orbital of O^{2-}) to an isolated Zr^{4+} (4d) ion in a tetrahedral configuration of Zr–O–P coordination,^{24,39} and the band gap for both samples is almost the same, ~ 5.20 eV (shown in the Supporting Information, Figure S5). Furthermore, the peak at the longer wavelength region (~ 300 nm) could be due to the interactions of Zr(IV) cations with the phosphate counteranions in the mesoporous framework.⁴⁰

4.6. Framework Vibrations. FT-IR spectra of the calcined mesoporous MZrP samples are shown in Supporting Information, Figure S6. The absence of the bands at ~ 2854 and ~ 2925 cm^{-1} for the calcined samples, which are ascribed to symmetric and asymmetric vibrations of the C–H groups, indicates the complete removal of F127 molecules from the as-synthesized materials after calcinations. The broad bands ~ 3500 and 1650 cm^{-1} are attributed to the asymmetric OH stretching and bending of the water molecule, respectively.⁴¹ Both the samples show absorption bands at 1000 – 1100 cm^{-1} corresponding to P–O stretching vibration and bands at ~ 2355 cm^{-1} due to the (P)–OH stretching vibration.^{32,42} The absence of phosphoryl (P=O) peaks at 1300 – 1400 cm^{-1} suggests the absence of PO_4^{3-} in the samples and also no distinct bands around 750 cm^{-1} , which could correspond to P–O–P deformation vibrations. The bands 527 cm^{-1} could be attributed to deformation modes of P–O–H.^{43,44}

4.7. Pyridine-IR. Pyridine adsorbed FT IR spectra of the calcined mesoporous zirconium oxophosphate materials show sharp bands at 1637 cm^{-1} and 1543 cm^{-1} (shown in Figure 5A), which are the characteristic bands of the typical pyridinium ion (PyH^+) confirming the presence of Brønsted acid sites.¹¹ This Brønsted acidity within the catalysts could be due to the presence of a reasonable amount of geminal $P(OH)_2$ and defect $P(OH)$ groups in the mesoporous zirconium oxophosphate frameworks.⁴⁵ Further, the band at 1490 cm^{-1} , which could be attributed to the adsorption of pyridine in Brønsted and Lewis sites at the same times is also present in these mesoporous samples (Figure 5A).¹¹ In sample 2 the band at about 1445 cm^{-1} , corresponding to the adsorbed pyridine at the Lewis acid site (PyL) is clearly observed, whereas that for samples 1 and 3 was very weak. Interestingly sample 3 prepared with less amount of phosphate (Zr/P = 4) showed very poor adsorption peaks suggesting very poor acidity of the material. In variable temperature FT IR analysis, the

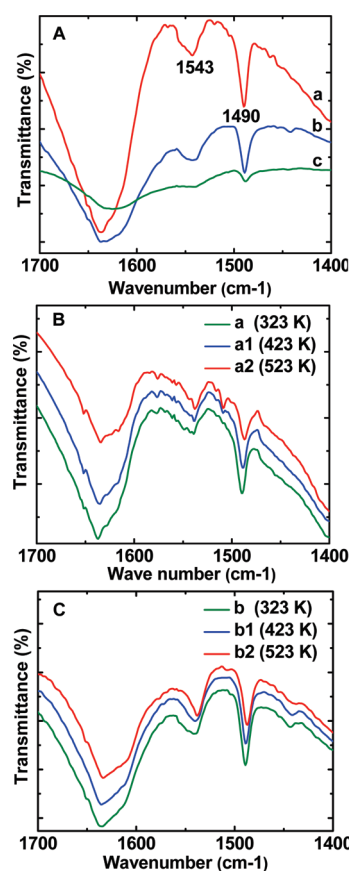


Figure 5. (A) FT–IR spectra of pyridine adsorbed samples 1 (a), 2 (b), and 3 (c) at room temperature. (B) FT–IR spectra of pyridine desorbed sample 1 at 323 K (a), 423 K (a1), and 523 K (a2). (C) FT–IR spectra of pyridine desorbed sample 2 at 323 K (b), 423 K (b1), and 523 K (b2).

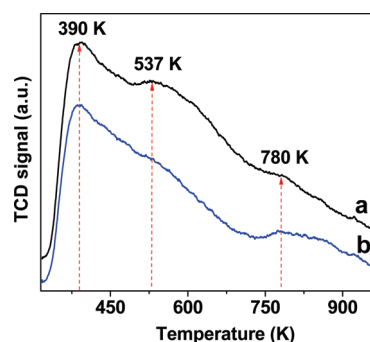
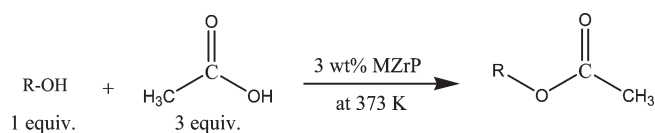


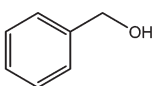
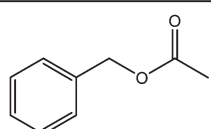
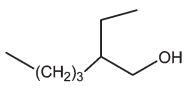
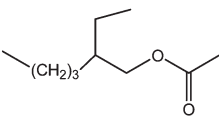
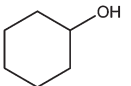
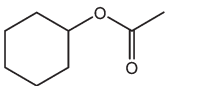
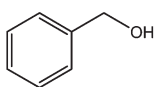
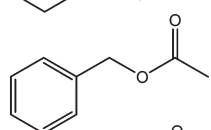
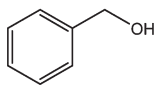
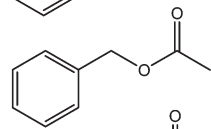
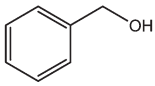
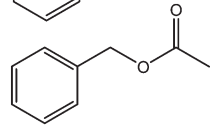
Figure 6. NH_3 -TPD profile over calcined mesoporous samples 1 (a) and 2 (b).

intensity of 1445 cm^{-1} and 1490 cm^{-1} bands gradually decrease with the increase of temperature, whereas the intensity of the 1543 cm^{-1} band remains almost identical, which demonstrates that the Lewis acid sites are relatively weak compared to the Brønsted acid sites (Figures 5B and 5C).

4.8. NH_3 -TPD. The acidic properties of calcined MZrP samples were investigated by temperature-programmed desorption of ammonia analysis, and the results are shown in Figure 6. Both samples show three distinct broad peaks due to the presence of weak, medium, and strong acid sites.^{46–48} The strength of the

Table 3. Esterification Reaction of Different Alcohols with Acetic Acid Catalyzed by Mesoporous Zirconium Oxophosphate Materials^a

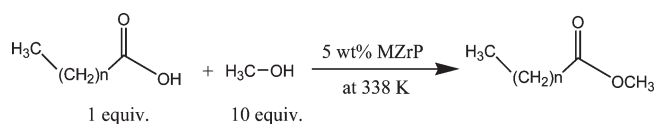


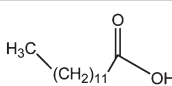
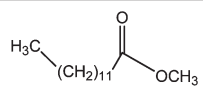
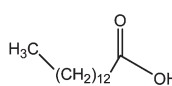
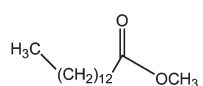
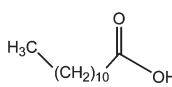
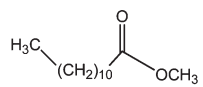
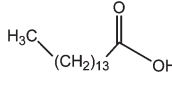
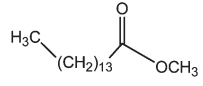
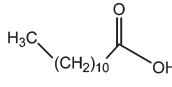
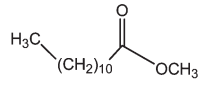
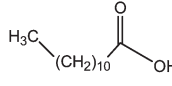
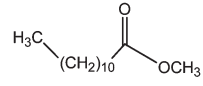
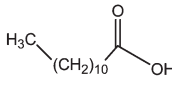
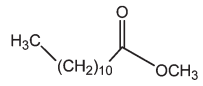
Entry	Substrate	Conversion	Product	TON
1		91.0		222
2		84.5		159
3		46.9		115
4 ^b		40.0		150
5 ^c		34.0		145
6 ^d		4.7		-

^a Reaction conditions: The esterification of alcohols with acetic acid was carried out with a mole ratio of alcohol/acetic acid of 1:3. Here acetic acid acts as reactant as well as solvent. Temperature of the reaction was maintained at 373 K. Catalyst was taken 3% (w/w) based on alcohol. TON (turn over number) = moles of substrate converted/mol of acid site of catalyst (estimated from the NH₃-TPD). ^b Esterification reaction was carried out with sample 2 as catalyst. ^c Esterification reaction was carried out with sample 3 as catalyst. ^d Esterification reaction was carried out without catalyst. In every case product selectivity is 100% and conversions of all the products were measured after 6 h reaction time.

acid site can be related to the corresponding desorption temperature. Sample 1 shows a little higher intensity and desorption in the temperature range of 363–435 K indicating higher number of weak acid sites than sample 2. Furthermore, from the figure it is clear that the medium strength acid sites are much higher for sample 1 than for sample 2. The higher amount of weak and medium acid sites in sample 1 is mainly due to the presence of high phosphate content within the mesoporous framework. High phosphate content could be responsible of geminal P(OH)₂ sites. Furthermore, both samples showed the presence of strong acid sites, as their respective desorption temperatures are quite high (737–835 K). Total acidity (calculated from total area under the peaks) for MZrP samples 1 and 2 are

Table 4. Esterification Reaction of Different Long-Chain Free Fatty Acids with Methanol Catalyzed by Mesoporous Zirconium Oxophosphate Materials^a



Entry	Substrate	Conversion %	Product	TON
1		86.4		56
2		74.8		43
3		72.0		53
4		70.8		37
5 ^b		40.6		46
6 ^c		33.0		44
7 ^d		3.7		-

^a Reaction conditions: The esterification of long-chain fatty acids with methanol was carried out with a mole ratio of fatty acid/methanol of 1:10. Here methanol acts as reactant as well as solvent. Temperature at of the reaction was maintained at 338 K. Catalyst was taken as 5% (w/w) based on fatty acid. ^b Esterification reaction was carried out with sample 2 as catalyst. ^c Esterification reaction was carried out with sample 3 as catalyst. ^d Esterification reaction was carried out without catalyst. In every case product selectivity is 100% and conversion of all the products were measured after 10 h.

30.63 and 20.03 cm³ g⁻¹, respectively. Thus, this result suggests that with an increase in Zr:P molar ratio from sample 1 to 2, the surface acidity for the mesoporous zirconium oxophosphate framework decreased. The decrease in total acidity from MZrP sample 1 to 2 in the NH₃-TPD study could be attributed to the lowering of surface area and phosphorus content in the mesoporous frameworks. During biodiesel synthesis through the heterogeneous esterification reaction, acid sites of the solid acid catalysts play a crucial role and as a result sample 1 should show better catalytic efficiency than sample 2. This trend is similar to that observed for zeolites, wherein the acid strength is higher at higher Si/Al ratio because of the larger number of isolated Al sites in the silica framework.⁴⁹

4.9. Catalytic Study. The catalytic performance of mesoporous zirconium oxophosphate with different $n_{\text{Zr}}/n_{\text{P}}$ ratio in

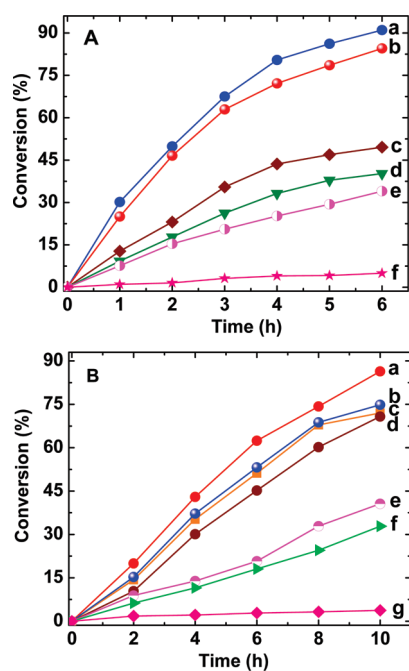


Figure 7. (A) Kinetic plots of esterification of different alcohols with acetic acid (a) benzyl alcohol, (b) 2-ethylhexanol, (c) cyclohexanol by using sample 1, (d) benzyl alcohol by using sample 2, (e) benzyl alcohol by using sample 3, and (f) benzyl alcohol without catalyst. (B) Kinetic plots of esterification of different long-chain free fatty acids with methanol (a) myristic acid, (b) palmitic acid, (c) lauric acid, (d) stearic acid by using sample 1, (e) lauric acid by using sample 2, (f) lauric acid by using sample 3, and (g) lauric acid without catalyst.

biodiesel synthesis was investigated in the esterification of different alcohols with acetic acid and several long-chain free fatty acids with methanol. Large amount of Bronsted acid sites at the catalyst surface usually favors this reaction.⁵⁰ Catalytic activity of the mesoporous zirconium oxophosphates are shown in the Tables 3 and 4, respectively. The kinetic plots of esterification of different alcohols with acetic acid and several long-chain free fatty acids with methanol are given in Figures 7A and 7B, respectively. Mesoporous zirconium oxophosphate (sample 1) showed excellent catalytic efficiency in the esterification of long-chain fatty acids with methanol. Only 3 wt % catalysts with respect to free fatty acids are sufficient to catalyze this reaction at 338 K. The calculated conversion of free fatty acids to the respective fatty acid methyl esters is based on the 100% selectivity. Sample 1 showed very good catalytic performance in the esterification of lauric, myristic, palmitic, and stearic acid with methanol, and conversion are 74.4%, 86.41%, 75.5%, and 74.2%, respectively, as shown in Table 4. Sample 2 showed little lower catalytic activity. From the results it is clear that decreasing the n_p/n_{Zr} ratio decreases the conversion of the fatty acids, which may be due to the lowering of surface area as well as surface acidity. Decrease in surface area thus in turn reflects the lowering of the number of active sites and thus lowers the rate of the catalytic reaction.

On the other hand the esterification reaction of different alcohols with acetic acid (shown in Table 3) show up to 91% conversion of benzyl alcohol within 6 h at 373 K. Whereas, 2-ethylhexanol and cyclohexanol show 84.5% and 47% conversion, respectively within 6 h under identical reaction conditions. The turn over numbers (TONs) for sample 1 in these reactions are quite high, indicating the catalyst is very much an efficient one. However, when we use

Scheme 1. Schematic Diagram of Catalytic Cycle during Esterification Reaction by Using Mesoporous Zirconium Oxophosphate Catalyst

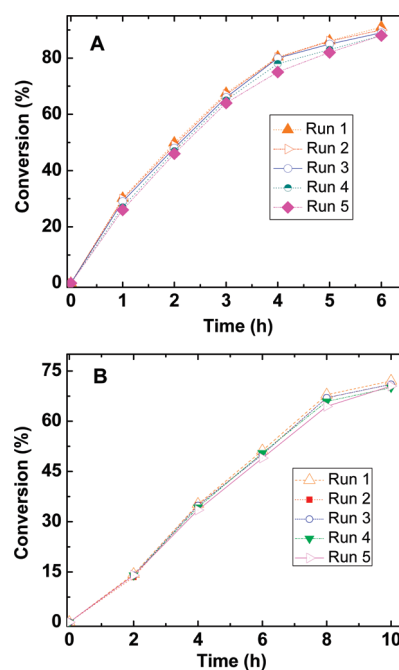
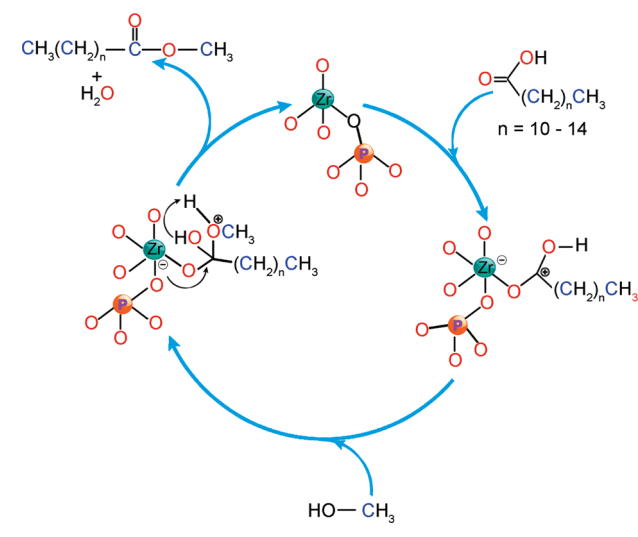


Figure 8. (A) Kinetic plots of recycling test of catalyst (sample 1) in the esterification reaction of alcohols with acetic acid, here benzyl alcohol has been taken as standard. (B) Kinetic plots of recycling test of catalyst (sample 1) in the esterification reaction of long-chain free fatty acids with methanol, here lauric acid has been taken as standard.

sample 2 (n_p/n_{Zr} ratio 1:1.51) as catalyst in the esterification of benzyl alcohol under similar reaction conditions the conversion decreases from 91% to only 40%. This could be attributed to the decrease in surface area and acid density. The proposed mechanism for the catalytic reaction shown in Scheme 1, where the initiation of the reaction could proceed through the attack of the carboxylic oxygen to the Zr center of the catalysts, results in carbocation formation. This carbocation then binds to the alcoholic oxygen, and

Table 5. Comparative Catalytic Performance of Reported Bio-Diesel Catalysts with Our Materials

entry	catalyst	fatty acid	alcohol: fatty acid	catalyst (wt %)	temp (K)	time (h)	conv.	ref.
1	Ta ₂ O ₅ /SiO ₂ -[H ₃ PW ₁₂ O ₄₀ (10.0)/Ph(3)]	palmitic acid	100	2	338	24	40.9	1
2	Zr-MCM-41	oleic acid	67	18.7	338	24	90	2
3	SiO ₂ -SZ (2, 0.5S)	lauric acid	10	20	341	6	38.1	12
4	SiO ₂ -SZ (2, 0.5S)	palmitic acid	10	20	341	6	39.4	12
5	SiO ₂ -SZ (2,1S)	palmitic acid	10	20	341	6	89.2	12
6	porous ZrP	palmitic acid	10	10	358	6	20	13
7	SBA-15-SO ₃ H	15 wt % palmitic acid	20	10	358	3	84	2
8	nafion	15 wt % palmitic acid	20	10	358	3	60	2a
9	sample 1	palmitic acid	10	5	338	10	86.4	this work
10	sample 1	lauric acid	10	5	338	10	72.0	this work

subsequent acid catalyzed elimination of water yields the desired ester.⁵¹

The stability as well as heterogeneous nature of mesoporous zirconium oxophosphate was investigated by performing a hot filtration test utilizing the sample 1 catalyst under the optimized reaction conditions. In this case the reaction was stopped when the conversion reached 30% and quickly removed the catalyst by filtration. The filtrate was immediately reused in the same reaction in an identical condition, and it was found that there was no further increase in substrate conversion. The filtered catalyst was also reused with fresh reagents after applying suitable conditions and negligible loss of its catalytic activity was observed. Further, when the reaction was carried out in the absence of catalyst, almost no conversion was found. These results confirmed that during the reaction no catalyst leaching occurs, and the reaction is a purely heterogeneous one in nature.^{9–12} The activity of a regenerated catalyst was inspected by filtration of the catalyst from an optimized reaction and then washing several times with methanol and anhydrous acetone followed by drying in an oven at 373 K overnight. The catalyst was subsequently activated at 673 K for 4 h under air flow and utilized for the above reaction. The same procedure was repeated an additional four times, and the kinetic plots for the conversion¹² in the esterification of different alcohols with acetic acid and several long-chain free fatty acids with methanol in the recycling process are shown in Figures 8A and 8B, respectively. The rate of conversion of different alcohols as well as different fatty acids into their corresponding products did not show any noticeable change during the progress of the reaction throughout five reaction cycles. Thus the mesoporous zirconium oxophosphate materials described herein have great potential to be a stable and highly active recyclable solid acid catalyst. In Table 5 we have provided a comparative catalytic performance of reported biodiesel catalysts with our mesoporous zirconium oxophosphate materials. Results suggested that our mesoporous zirconium phosphate material is a superior catalyst for the production of biodiesel over the existing catalysts known in the literature (Table 5).

5. CONCLUSION

In conclusion, we have presented the synthesis of new mesoporous zirconium oxophosphates through the EISA method using a non-ionic amphiphilic triblock copolymer surfactant, pluronic F127 under acidic pH conditions. TEM and N₂ adsorption/desorption studies established the mesoporous nature of these materials. Spectroscopic results suggested that most

of the zirconium sites present in these samples are tetrahedrally coordinated Zr(IV). In addition to tetrahedral coordination there is considerable extent of five or six coordinated zirconium present in the extra-framework of the materials, which could result because of its synthesis under strong acidic conditions. NH₃-TPD analysis suggests the presence of Lewis and Brønsted acid sites, and pyridine adsorbed FT IR spectral studies also confirm this observation. The high acid density and large surface area could be employed for an efficient biodiesel catalyst. Furthermore, large pore size that favors the diffusion of large organic molecules contributes to the enhancement of catalytic ability. These catalysts efficiently converted the long chain fatty acids to their corresponding methyl ester with methanol as well as different alcohols to their corresponding ester with glacial acetic acid. In a typical reaction the observed biodiesel yield was over 91% under an optimal reaction conditions. Moreover, this mesoporous solid acid catalyst has been recycled five times with negligible loss of activity, suggesting high chemical stability and reusability of the mesoporous zirconium oxophosphate framework.

■ ASSOCIATED CONTENT

Supporting Information. Wide angle PXRD, FE-SEM images, UV–vis diffuse reflectance spectrum, Nitrogen adsorption/desorption isotherms and corresponding pore size of sample 1 and sample 2 calcined at 1173 K, band gap, FT IR and TG-DTA profile have been given. This material is available free of charge via the Internet at <http://pubs.acs.org>.

■ AUTHOR INFORMATION

Corresponding Author

*E-mail: msab@iacs.res.in.

■ ACKNOWLEDGMENT

S.K.D. and M.K.B. wish to thank CSIR, New Delhi for their respective Senior Research Fellowships.

■ REFERENCES

- (1) Wang, W.; Chen, C. L.; Xu, N. P.; Mou, C. Y. *Green Chem.* **2002**, *4*, 257–260.
- (2) Tao, Y. S.; Kanoh, H.; Abrams, L.; Kaneko, K. *Chem. Rev.* **2006**, *106*, 896–910.
- (3) Li, W.; Choi, S.; Drese, J. H.; Hornbostel, M.; Krishnan, G.; Eisenberger, P. M.; Jones, C. W. *ChemSusChem* **2010**, *3*, 899–903.

- (4) Mbaraka, I. K.; Shanks, B. H. *J. Catal.* **2003**, *219*, 329–336.
- (5) Mbaraka, I. K.; Radu, D. R.; Lin, V. S.; Shanks, B. H. *J. Catal.* **2003**, *219*, 365–373.
- (6) Liu, D.; Bhan, A.; Tsapatsis, M.; Hashimi, S. A. *ACS Catal.* **2011**, *1*, 7–17.
- (7) Dimian, A. C.; Srokol, Z. W.; Mittelmeijer-Hazeleger, M. C.; Rothenberg, G. *Top. Catal.* **2010**, *53*, 1197–1201.
- (8) Liu, R.; Wang, X.; Zhao, X.; Feng, P. *Carbon* **2008**, *46*, 1664–1669.
- (9) Jones, C. W.; Tsuji, K.; Davis, M. E. *Nature* **1998**, *393*, 52–54.
- (10) Tanabe, K.; Hoelderich, W. F. *Appl. Catal., A* **1999**, *181*, 399–436.
- (11) Sinhamahapatra, A.; Sutradhar, N.; Roy, B.; Tarafdar, A.; Bajaj, H. C.; Panda, A. B. *Appl. Catal., A* **2010**, *385*, 22–30.
- (12) Jones, C. W. *Top. Catal.* **2010**, *53*, 942–952.
- (13) Di Serio, M.; Tesser, R.; Pengmei, L.; Santacesaria, E. *Energy Fuels* **2008**, *22*, 207–217.
- (14) Kouzu, M.; Yamanaka, S.; Hidaka, J.; Tsunomori, M. *Appl. Catal., A* **2009**, *355*, 94–99.
- (15) Ma, F.; Hanna, M. A. *Bioresour. Technol.* **1999**, *70*, 1–15.
- (16) Lotero, E.; Liu, Y.; Lopez, D. E.; Suwannakarn, K.; Bruce, D. A.; Goodwin, J. G. *Ind. Eng. Chem. Res.* **2005**, *44*, 5353–5363.
- (17) Macarioa, A.; Giordanoa, G.; Onida, B.; Cocina, D.; Tagarelli, A.; Giuffrè, A. M. *Appl. Catal., A* **2010**, *378*, 160–168.
- (18) Kirumakki, S. R.; Nagaraju, N.; Chary, K. V. R. *Appl. Catal., A* **2006**, *299*, 185–192.
- (19) Liu, Y.; Lotero, E.; Goodwin, J. G., Jr.; A. *J. Catal.* **2006**, *242*, 278–286.
- (20) Kulkarni, M. G.; Gopinaht, R.; Meher, L. C.; Dalai, A. K. *Green Chem.* **2006**, *8*, 1056–1062.
- (21) Kiss, A. A.; Dimian, A. C.; Rothenberg, G. *Adv. Synth. Catal.* **2006**, *348*, 75–81.
- (22) Kiss, A. A.; Dimian, A. C.; Rothenberg, G. *Energy Fuels* **2008**, *22*, 598–604.
- (23) Kiss, A. A.; Omata, F.; Dimian, A. C.; Rothenberg, G. *Top. Catal.* **2006**, *40*, 141–150.
- (24) Chen, X.-R.; Ju, Y.-H.; Mou, C.-Y. *J. Phys. Chem. C* **2007**, *111*, 18731–18737.
- (25) Fang, D.; Yang, J.; Jiao, C. *ACS Catal.* **2011**, *1*, 42–47.
- (26) Rao, K. N.; Sridhar, A.; Lee, A. F.; Tavener, S. J.; Young, N. A.; Wilson, K. *Green Chem.* **2006**, *8*, 790–797.
- (27) Feng, Y. F.; Yang, X. Y.; Yang, D.; Du, Y. C.; Zhang, Y. L.; Xiao, F. S. *J. Phys. Chem. B* **2006**, *110*, 14142–14147.
- (28) Bhaumik, A.; Inagaki, S. *J. Am. Chem. Soc.* **2001**, *123*, 691–696.
- (29) Tian, B. Z.; Liu, X. Y.; Tu, B.; Yu, C. Z.; Fan, J.; Wang, L. M.; Xie, S. H.; Stucky, G. D.; Zhao, D. Y. *Nat. Mater.* **2003**, *2*, 159–163.
- (30) Ciesla, U.; Fröba, M.; Stucky, G.; Schüth, F. *Chem. Mater.* **1999**, *11*, 227–234.
- (31) Kleitz, F.; Thomson, S. J.; Liu, Z.; Terasaki, O.; Schüth, F. *Chem. Mater.* **2002**, *14*, 4134–4144.
- (32) Wu, P.; Liu, Y.; He, M.; Iwamoto, M. *Chem. Mater.* **2005**, *17*, 3921–3928.
- (33) Jacobson, K.; Gopinath, R.; Meher, L. C.; Dalai, A. K. *Appl. Catal., B* **2008**, *85*, 86–91.
- (34) Paul, M.; Pal, N.; Rana, B. S.; Sinha, A. K.; Bhaumik, A. *Catal. Commun.* **2009**, *10*, 2041–2045.
- (35) Yuan, Z.-Y.; Ren, T.-Z.; Azioune, A.; Pireaux, J.-J.; Su, B.-L. *Catal. Today* **2005**, *105*, 647–654.
- (36) Boissière, C.; Larbot, A.; van der Lee, A.; Kooyman, P. J.; Prouzet, E. *Chem. Mater.* **2000**, *12*, 2902–2913.
- (37) Das, S. K.; Bhunia, M. K.; Bhaumik, A. *Dalton Trans.* **2010**, *39*, 4382–4390.
- (38) Mal, N. K.; Bhaumik, A.; Fujiwara, M.; Matsukata, M. *Microporous Mesoporous Mater.* **2006**, *93*, 40–45.
- (39) Kapoor, M. P.; Inagaki, S.; Yoshida, H. *J. Phys. Chem. B* **2005**, *109*, 9231–9238.
- (40) Ziyada, M.; Rouimia, M.; Portefaixb, J. L. *Appl. Catal., A* **1999**, *183*, 93–105.
- (41) Nishiyama, Y.; Tanaka, S.; Hillhouse, H. W.; Nishiyama, N.; Egashira, Y.; Ueyama, K. *Langmuir* **2006**, *22*, 9469–9472.
- (42) Kim, H. N.; Keller, S. W.; Mallouk, T. E.; Schmitt, J.; Decher, G. *Chem. Mater.* **1997**, *9*, 1414–1421.
- (43) Tian, X.; He, W.; Cui, J.; Zhang, X.; Zhou, W.; Yan, S.; Sun, X.; Han, X.; Han, S.; Yue, Y. *J. Colloid Interface Sci.* **2010**, *343*, 344–349.
- (44) Jiménez-Jiménez, J.; Maireles-Torres, P.; Olivera-Pastor, P.; Rodríguez-Castellón, E.; Jiménez-López, A.; Jones, D. J.; Rozière, J. *Adv. Mater.* **1998**, *10*, 812–815.
- (45) Corma, A. *Chem. Rev.* **1995**, *95*, 559–614.
- (46) Das, S. K.; Bhunia, M. K.; Sinha, A. K.; Bhaumik, A. *J. Phys. Chem. C* **2009**, *113*, 8918–8923.
- (47) Paul, M.; Pal, N.; Rajamohan, P. R.; Rana, B. S.; Sinha, A. K.; Bhaumik, A. *Phys. Chem. Chem. Phys.* **2010**, *12*, 9389–9394.
- (48) Zhang, J.; Ma, Z.; Jiao, J.; Yin, H.; Yan, W.; Hagaman, E. W.; Yu, J.; Dai, S. *Microporous Mesoporous Mater.* **2010**, *129*, 200–209.
- (49) Teraishi, K.; Akanuma, K. *J. Phys. Chem. B* **1997**, *101*, 1298–1304.
- (50) Zabeti, M.; Daud, W. M. A. W.; Aroua, M. K. *Fuel Process. Technol.* **2009**, *90*, 770–777.
- (51) Lam, M. K.; Lee, K. T.; Mohamed, A. R. *Biotechnol. Adv.* **2010**, *28*, 500–518.